Ann. Geophysicae 17, 1182–1198 (1999) © EGS – Springer-Verlag 1999

Annales Geophysicae

On the usefulness of *E* region electron temperatures and lower *F* region ion temperatures for the extraction of thermospheric parameters: a case study

J.-P. St.-Maurice[1], **C. Cussenot**[2], **W. Kofman**[2]

[1] Department of Physics and Astronomy, The University of Western Ontario, London, Ontario N6A 3K7, Canada
[2] LIS, URA 342, BP-46, 38402 Saint Martin d'hères Cedex, France

Received: 21 October 1998 / Revised: 20 January 1999 / Accepted: 3 February 1999

Abstract Using EISCAT data, we have studied the behavior of the *E* region electron temperature and of the lower *F* region ion temperature during a period that was particularly active geomagnetically. We have found that the *E* region electron temperatures responded quite predictably to the effective electric field. For this reason, the *E* region electron temperature correlated well with the lower *F* region ion temperature. However, there were several instances during the period under study when the magnitude of the *E* region electron temperature response was much larger than expected from the ion temperature observations at higher altitudes. We discovered that these instances were related to very strong neutral winds in the 110–175 km altitude region. In one instance that was scrutinized in detail using *E* region ion drift measurement in conjunction with the temperature observations, we uncovered that, as suspected, the wind was moving in a direction closely matching that of the ions, strongly suggesting that ion drag was at work. In this particular instance the wind reached a magnitude of the order of 350 m/s at 115 km and of at least 750 m/s at 160 km altitude. Curiously enough, there was no indication of strong upper *F* region neutral winds at the time; this might have been because the event was uncovered around noon, at a time when, in the *F* region, the $\mathbf{E} \times \mathbf{B}$ drift was strongly westward but the pressure gradients strongly northward in the *F* region. Our study indicates that both the lower *F* region ion temperatures and the *E* region electron temperatures can be used to extract useful geophysical parameters such as the neutral density (through a determination of ion-neutral collision frequencies) and Joule heating rates (through the direct connection that we have confirmed exists between temperatures and the effective electric field).

Key words. Ionosphere (auroral ionosphere; ionosphere atmosphere interactions; plasma temperature and density)

1 Introduction

It has been repeatedly pointed out that the ion temperature below 400 km altitude depends quadratically on the magnitude of the relative drift between ions and neutrals (e.g., Rees and Walker, 1968; St.-Maurice and Hanson, 1982, 1984). However, it may not have been stressed strongly enough that this is equivalent to the ion temperature having a quadratic dependence on the magnitude of the effective electric field $\mathbf{E}' = \mathbf{E} + \mathbf{V}_n \times \mathbf{B}$. Thayer (1998a, b) recently emphasized that the actual Joule heating rate that determines a large fraction of the rate at which energy is transferred from the magnetosphere to the thermosphere actually depends on the magnitude of the effective electric field through $\int \sigma_P(z)|E'|^2 dz$ where z is the altitude and σ_P is the height-dependent Petersen conductivity. The ion temperatures obtained with incoherent scatter radars should therefore in principle, provide an accurate description of the Joule heating rates without even the need for drift measurements. However, as we discuss in more detail below, things are not so simple: on the one hand, the temperature enhancements have to be large enough to avoid large uncertainties associated with neutral temperature models and error bars on the measurements. On the other hand, when the temperature enhancements are large, the ion velocity distribution becomes anisotropic and non-Maxwellian which complicates the analysis sometimes considerably. For these reasons, the ion temperatures may have been overlooked as a useful tool for monitoring the state of the thermosphere. But with considerable progress made on data processing and analysis together with a much

Correspondence to: J.-P. St.-Maurice

clearer characterization of non-Maxwellian features the time has come to give the ion temperature another shot.

A similar situation has evolved with electron temperatures in the *E* region. As we discuss in more detail below, it is now clear that for electric fields of the order of 40 mV/m or greater the electron temperature rapidly climbs up well above the neutral and ion temperatures. Much emphasis has been given to producing an expression for the heating rates using nonlinear plasma physics, at the expense of exploring the possibilities that the enhancements can provide as a tool to study the thermosphere. Later in this paper we show that one can argue on theoretical grounds that the electrons, like the ions, respond to the effective electric field rather than to the electric field itself. This would imply that the electrons could be used to monitor the Joule heating rates in an altitude range that is particularly important for magnetospheric energy deposition rates. Again, we wish to argue here that knowledge and technology have now both progressed to the point that this is entirely feasible.

One of the features that may have hindered progress in terms of utilizing electron temperatures is that, contrary to what has been obtained with small data subsets over several hours of data acquisition, the electron temperature data often exhibit a large amount of scatter when plotted against the electric field strength. This has been blamed in the past mostly on poor electric field estimates (St.-Maurice *et al.*, 1990; Haldoupis *et al.*, 1993; Williams *et al.*, 1992). Since many radar experiments do not monitor the electric fields on as short a time-scale as the temperatures, this may have led to a lack of study of many a data set. It may be, however, that much of the scatter in T_e versus electric field plots is actually of a geophysical rather than statistical nature. One is reminded of a similar problem that was faced by St.-Maurice and Hanson (1984) when looking at large data sets of ion temperatures onboard the AE-C satellite: as the electric field was increasing the ion temperatures would exhibit increasingly large standard deviations about a mean that was close to the values expected for zero neutral winds. The source of the scatter was identified with neutral wind values of fairly normal magnitudes affecting the temperature response through simple changes in the angle between winds and ion drifts. Given that there is a strong theoretical case for the electron temperature to also respond to the effective electric field and not the field itself one is left wondering about that possibility for the *E* region electron temperatures as well.

Our most important goal in this paper is therefore to document the effective electric field dependence of the *E* region electron temperature based on EISCAT radar observations of the phenomenon. To this end we will present results from 24 h of data acquired during an extremely geomagnetically disturbed period. In the process of making our case, we will also show that the behavior of the ion temperature is now understood well enough to extract reliable values for the effective electric field throughout the upper *E* region and the lower *F* region. We will in fact show how the ion-neutral collision frequency can be extracted from the ion temperature and drift behavior in the *E* region, implying that once calibrated, the electron temperatures below 120 km could be used to extract this information more easily and quite reliably during heating events. Finally, we will also present, using the principles we uncovered, one example for which we extracted neutral winds of exceptional magnitudes in the *E* region and lower *F* region. The data in that case was strongly indicative of a strong ion drag effect, which did not seem, however, to extend to upper *F* region heights.

Before presenting our particular data set and our analysis of it we will review briefly in sect. 2 the basis for using ion and electron temperatures as proxies for the effective electric field strength. This is followed in sect. 3 by a description of the particular experiment that we used and an overview of the data that were acquired. In sect. 4 we focus on a rather striking feature of our particular data set in which an 'upper electron temperature branch' (UTEB) clearly emerges from the rest of the data. From a detailed study of the available data during UTEB events we will show that very strong *E* region neutral winds were affecting both the ion and the electron temperature data, but more so the ions above 130 km altitude. Further evidence that this was indeed the case is presented in sect. 5, where we have extended our method to include the observation of ion drift vectors during a particular time interval for which the electric field did not change.

2 The connection between ion and electron temperatures and the effective electric field strength

2.1 Ions

The dominant terms in the ion energy balance below 400 km altitude are the frictional heating term and the heat exchange term with the neutrals. The lower the altitude the truer this becomes. The equation that results from this balance is, to a good approximation, given by (e.g., St.-Maurice and Hanson, 1982)

$$T_i = T_n + \frac{\langle m_n \rangle}{3K_b}(\mathbf{V}_i - \mathbf{V}_n)^2 \tag{1}$$

where T_i and T_n are the ion and neutral temperatures respectively, K_b is the Boltzmann constant, $\mathbf{V}_i$ and $\mathbf{V}_n$ are the ion and neutral drifts respectively and $\langle m_n \rangle$ is a collision-frequency-weighted average neutral mass.

We can also write T_i in terms of the effective electric field $\mathbf{E}' = \mathbf{E} + \mathbf{V}_n \times \mathbf{B}$. As we show in the Appendix, Eq. (1) can then be replaced by

$$T_i = T_n + \frac{\langle m_n \rangle}{3K_b}\frac{(\mathbf{E}'/B)^2}{1+\alpha_i^2} \tag{2}$$

where $\alpha_i = \nu_i/\Omega_i$ is the ion collision to cyclotron frequency ratio. The merit of Eq. (2) is to express explicitly that T_i depends strictly on the effective electric field, and not on the electric field itself.

Equation (2) implies that, to obtain the magnitude of the effective electric field and its altitude variation, one "simply" has to study the variation of T_i with altitude. Things are not quite that straightforward in practice, however; even with an ideal situation where radar spectra would have excellent signal-to-noise ratio, there are several difficulties to wrestle with. For one thing both T_n and $\langle m_n \rangle$ are altitude-dependent, particularly between 175 and 225 km, where the dominant neutral switches from N_2 to O while T_n undergoes a transition from radiation-dominated to heat-flow-dominated. To make things worse, during active conditions, Joule heating effects lead to increases in the neutral temperatures and to increases in the average N_2 to O composition ratio, at all F region heights. This all conspires to make an accurate description of the altitude dependence of T_i much more difficult in the altitude transition region where the dominant neutral switches from N_2 to O.

Another complication, which becomes important when the electric field is large, is that the ionospheric ion temperature becomes anisotropic and the ion velocity distribution becomes non-Maxwellian, with a larger temperature value perpendicular versus along the magnetic field direction (e.g., Gaimard *et al.*, 1998). Therefore, if, as will be the case here, one is to use measurements made along the magnetic field to determine the ion temperature, one has to remember that the line-of-sight temperature will actually be smaller than the average ion temperature given by Eqs. (1) or (2). Specifically, the parallel temperature can be adequately described by the equation

$$T_{i\|} = T_n + \frac{\langle m_n \rangle}{3K_b} \frac{(\mathbf{E}'/B)^2}{1+\alpha_i^2} 1.5\beta_{\|} \tag{3}$$

Unfortunately, the value of $\beta_{\|}$ changes significantly both with ion and neutral composition. For the N_2 dominated atmosphere below 175 km we will be following McCrea *et al.* (1993) and use $\beta_{\|} \approx 0.52$ (as opposed to 2/3 for a spherically symmetric distribution). From the same work, but for the oxygen-dominated atmosphere above 250 km, $\beta_{\|}$ should be between 0.18 and 0.25 when dealing with O^+ ions. Note that the $\beta_{\|}$ difficulties notwithstanding, the parallel ion temperature still theoretically increases quadratically to first order with the effective electric field strength.

There remains the actual non-Maxwellian shape of the ion velocity distribution to deal with. This affects the radar spectra and is more difficult to model because the spectral shape is a function of both the electron-to-ion temperature ratio and of the ion mass. Both change with altitude but unfortunately in a somewhat unpredictable manner, particularly at high latitudes. Nevertheless, using theoretical and Monte-Carlo calculations, it has been shown that the non-Maxwellian spectra can be inverted particularly if the signal to noise is of good quality and if the angle between the line of sight and the magnetic field is not too steep (e.g., Winkler *et al.*, 1992; Hubert and Lathuillere, 1989). It also helps to be in situation where N_2 is the dominant neutral constituent because in that case the departures from a Maxwellian shape are not as large nor as difficult to model as when the background neutral gas is O.

The above implies that it is easier to use the ion temperature to retrieve the magnitude of the effective electric field at altitudes ranging between 130 km and 175 km. The main reasons for this are (1) above 130 km α_i is small so that the magnitude of the temperature response is at its largest and (2) the dominant neutral atmospheric constituent in that case is N_2 for sure. The advantages of being in a region where N_2 is the dominant neutral are many: for one thing, a larger mean neutral mass, $\langle m_n \rangle$, increases the magnitude of the ion temperature response to the electric field (see Eq. 2). For another, it removes the uncertainty in the average neutral mass, which can be highly variable above 180 km in the auroral region and can therefore introduce modulations in the response of T_i to the effective electric field strength. And finally, the ion composition is also dominated by NO^+ ions when the neutrals are mostly N_2 (i.e., below 170 km for sure), which removes some further ambivalence with respect to the interpretation of non-Maxwellian ion line spectra. This being said, we will not go as far as to attempt to correct for non-Maxwellian distortions although we will consider anisotropic ion temperature effects. Our neglect of other non-Maxwellian distortions should not create a systematic effect, although it will admittedly be introducing some additional scatter in the data (e.g., Lathuillere and Hubert, 1989).

2.2 Electrons

Schlegel and St.-Maurice (1981) and Wickwar *et al.* (1981) discovered that, if the electric field strength exceeds about 40 mV/m at high latitudes, the electron temperature around 105–115 km is correlated with the electric field strength (while being generally anti-correlated with electron precipitation at those heights). These basic results were confirmed by many subsequent studies (see review by St.-Maurice *et al.* (1990) for papers prior to 1990; also see Jones *et al.*, 1991; Williams *et al.*, 1992; Haldoupis *et al.*, 1993) and are now accepted as a fact of life in high latitude ionospheric phenomenology.

The heating mechanism associated with the observed electron temperature enhancements has from the very beginning (Schlegel and St.-Maurice, 1981) been suspected to be due to the interaction of electrons with large amplitude plasma waves triggered by the Farley-Buneman instability. Two non-resonant heating mechanisms have been considered: one was described by Robinson (1986) as a form of frictional heating between electrons and the plasma waves and was linked to the notion of an anomalous electron collision frequency due to the waves. While this process has to be happening to a certain extent, it was argued in particular by St.-Maurice (1990) that the anomalous collision frequency inferred from the Robinson theory is much larger than would be suggested from wave-amplitude observations. St.-Maurice and co-workers therefore suggested instead that large amplitude waves were able to sustain electric fields

components along the magnetic field that are large enough to heat the electrons to produce the observed temperatures (e.g., St.-Maurice and Laher, 1985).

Whatever the detailed mechanism, one could look at the problem this way: in a steady-state situation, the power going through large amplitude plasma waves has to go back to particles. Since the power going to the waves is actually dominated by Joule dissipation even in the linear growth stages (St.-Maurice, 1987), one has to conclude that the electron heating rate should be related to the effective electric field at least quadratically once unstable waves are triggered (we show in the Appendix that the heating rate depends on the effective electric field even though the instability extracts its power from the currents). The heating rate may very well go up even faster because (1) the electron-neutral collision frequency, on which the heating rate depends linearly, also changes dramatically with the electron temperature itself and (2) an increasingly large range of unstable modes is excited as the ambient electric field increases (Kissack *et al.*, 1997). In other words, once it is recognized that the plasma waves can reach a large enough amplitude to heat the electrons, the heating rate can only increase rapidly (at least quadratically) with effective electric field strength. One more observation deserves a mention: since the effective electric field is not normally expected to change much with altitude below 115 km and since the heating and cooling rates are otherwise both proportional to the neutral density, the only reason why the electron temperature goes down at all as we go from 115 km down to 100 km is that the power going through the waves must also be going down. This is consistent with the fact that the linear growth rates are known to become smaller as we go down in altitude.

At any rate, as far as a precise quantitative description of the electron temperature is concerned our approach in the present paper will be similar to the one taken by St.-Maurice *et al.* (1990), namely, we will simply rely on the data itself to infer the relation between the electron temperature and the effective electric field strength.

3 Description and overview of the observations

The data were obtained during a 25-h UHF (980 MHz) EISCAT run that started at 10 UT on 9 April 1990. The Tromso radar, where the transmitter is located, recorded spectra along the magnetic field line for the duration of the experiment. A multipulse offering a 3-km resolution with 2.7-km range-stepping was used between 90 km and 250 km altitudes. A long pulse with a 22 km range step and 54 km altitude resolution was also used to cover the altitude range 150–600 km. For this paper we used a 1 min integration time with the analysis of the Tromso data.

The remote stations at Kiruna and Sodankyla were used in a scanning mode that intersected the Tromso geomagnetic field lines at seven particular altitudes: 90 km, 95.5 km, 100.5 km, 108 km, 116.2 km, 124 km and 278 km. The 278 km altitude gate provided a measurement of the plasma $\mathbf{E} \times \mathbf{B}$ drift vector while the lower altitudes were used to determine the ion drift in regions where the ions were unmagnetized or, at most, only partially magnetized. The altitude scan mode was such that the $\mathbf{E} \times \mathbf{B}$ drift could be sampled at 5-min intervals.

Below 108 km altitude, at the UHF frequency used for the data analysis presented here, the shape of the ion line spectrum is affected by ion-neutral collisions, which tend to drive a Lorentzian shape, as well as by the ratio T_e/T_i, which tends to drive a double-hump spectrum if $T_e > T_i$. It is not possible to solve for ion-neutral collisions and for the ratio T_e/T_i simultaneously. Instead, one either solves for the collision frequency assuming $T_e = T_i$, or one fixes the collision frequency and solves for the individual temperatures. In this latter case we use an empirical collision frequency model derived under similar conditions, but in the absence of strong electric field (Kofman *et al.*, 1986). We note that the essential quantitative results that we will present here will depend on the ion and electron temperatures obtained above 108 km anyway, so that any uncertainty introduced by the use of our empirical collision model will only have minimal impact on what we shall present.

A second factor could affect the data interpretation, namely, the ion composition. Unless a whole profile is being fitted, which is not the case here, we have to rely on a composition model to determine the ion temperature. This is because the spectrum basically yields the value of the thermal speed, which is proportional to $\sqrt{T_i/m_i}$ where m_i represents the mean ion mass. In the altitude range 150–250 km the ion goes from all molecular (NO^+) to basically all atomic (O^+). In order to avoid complications with composition uncertainties (which are compounded by chemical effects during ion heating events), we have limited our study for the most part to altitudes either greater than 250 km or less than 170 km, deriving the ion temperatures using a standard EISCAT composition model. This means that, for instance, at 168 km, we have assumed that the NO^+ to n_e density ratio was 0.83. During heating events associated with large electric fields, the molecular ion concentration should increase, and it is likely that the ratio will increase above 0.83. However, judging from statistical studies (Lathuillere and Pibaret, 1992) as well as a case study (Lathuillere, 1987) it seems very unlikely that at 168 km the ratio will exceed 0.90. For multipulse data, the related possible underestimation in T_i at 168 km will therefore be less than 15% for sure, and very likely be less than half that value in fact. However, for long pulse data centered on 168 km, the possible uncertainties will in principle be larger because of pulse smearing effects. This being said, a variation in excess of 15% still seems to be unlikely even in that case. Finally, for multipulse data lower down, also note that for altitudes 150 km and less, the composition model we used is already more than 95% NO^+ below 150 km altitude. This implies that the analyzed T_i is not affected by ion heating-induced composition changes in any major way below 150 km.

As a form of introduction for the work that we are about to present, we show in Fig. 1 how the magnitude

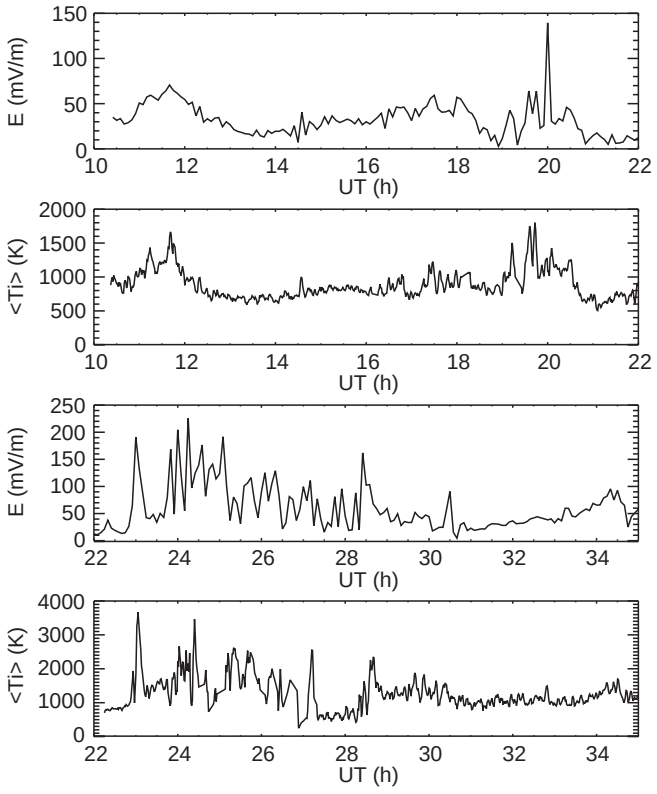

Fig. 1. Time series for 9–10 April 1990, of the electric field measured tristatically at 278 km altitude every 5 min and of the 1-minute average parallel ion temperature between 140 and 160 km altitudes using the multipulse mode

of the $\mathbf{E} \times \mathbf{B}$ drift sampled by the remote stations changed with time during the period of observation. For comparison, we also display on the same time-scale the behavior of the parallel ion temperature. The ion temperature was sampled every minute, which makes for the higher density of points. Also, because of the degree of noise associated with the multipulse we took an altitude average of the ion temperature between the 140 and 160 km altitude gates as well as a 3-point running-average in time. In spite of the smoothing brought by this procedure, there is little doubt that many of the $\pm 50K$ oscillations in the resulting plot are due to noise. Notice also that bad data points were excluded and that this led at times to larger jumps between points. Not surprisingly, there was a tendency for bad data points to be observed when the electric field was highly structured in time and the ion density was simultaneously small, resulting in autocorrelation functions that could not be satisfactorily fitted, probably because of poor signal-to-noise ratios.

Figure 1 illustrates that the electric field exceeded 100 mV/m on several occasions, particularly around midnight (around the time that the A_p index reached its maximum value of 207 for the event). The measured $\mathbf{E} \times \mathbf{B}$ drift actually exceeded 3 km/s on a few occasions and even went beyond 4 km/s in one case. This result is remarkable in that very strong electric fields are usually difficult to catch because of their high localization and short lifetime. As a result, it is quite reasonable to expect that particularly in the time interval 24:00–25:00 UT the field may well have reached or exceeded the 200 mV/m value on more than one occasion.

To show that the inference of very strong electric fields was indeed strongly supported by other features in the data, we present in Fig. 2 two profiles of the ion temperature for the long pulse data taken during the time interval over which the electric field was reaching very large values. As Fig. 2 shows, consistent with our expectations of exceptional electric fields, the long pulse data reported parallel ion temperatures in excess of 12,000 K below 200 km altitude in the examples shown. (Notice that the signal-to-noise ratio was too small for the multipulse to produce useful estimates during that time). At the times of the posted observations, the electric field estimated from the 278 km altitude ion drift measurement reached 225 mV/m (top panel) and 141 mV/m (bottom panel). Notice how the parallel ion temperature above 200 km was substantially less than lower down. This is mainly due to the mean mass factor in Eq. (1), which is dominated by N_2 below 175 km and by O above 200 km. A similar kind of ion temperature profile behavior under very strong electric field conditions was in fact reported earlier by Kofman and Lathuillere (1987).

Figure 1 illustrates that the selected experimental mode suffered some drawbacks when the electric field became very strong for the case under study. We refer here to the large point by point oscillations in the electric field data on the 5-min time-scale that could be observed particularly around 24:00 UT. These oscillations indicate that the strong electric fields were highly variable over the 5-min time-scale, and that it was risky at best to try to even interpolate the data to get the electric field variations on shorter time scales during that time period. This means that we had to fall back on the temperature measurements to monitor the magnitude of the electric field on shorter time scales. Thus, the ion temperatures obtained with the long pulse along the geomagnetic field line was not only giving a better temporal resolution, but was also better able to track the electric field strength than the drift measurements, at least during periods of reduced ion densities. This being said, one should note the general correlation between the parallel ion temperatures and the drift-deduced electric field strength in Fig. 1, as expected from Eqs. (1) or (3). Thus, there was general agreement between the two measurements, but some of the details differed. In our in-depth analysis, such details could be important, as we shall illustrate in sect. 4.

4 The detailed response of T_i and T_e to electric field variations

4.1 Results from scatter plots

For the reasons presented in sect. 2, both the ion temperature around 150–160 km altitude and the electron temperature in the *E* region could be expected to be good indicators of the electric field strength if, as is often

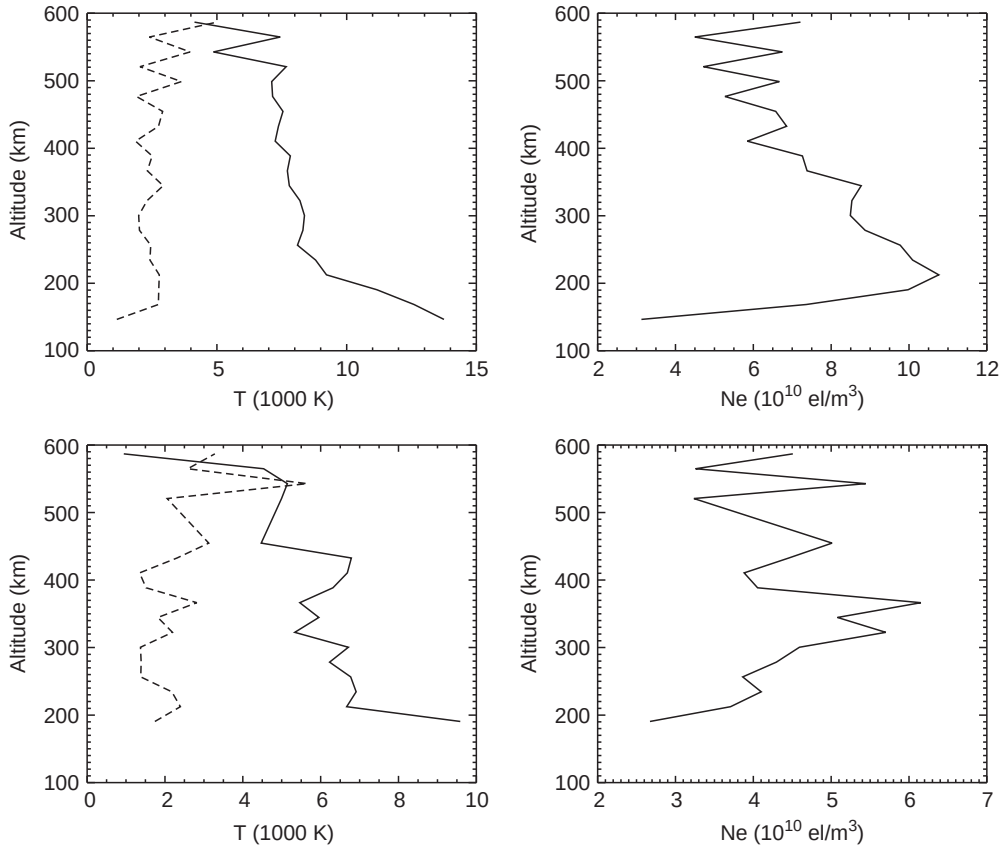

Fig. 2. Example of density (*right-hand-side*) and temperature profiles (*left-hand-side*) with much larger ion temperatures (*full lines*) than average. The electron temperatures are also shown on the *left-hand-side panels* (*dashed lines*). The times were taken in the middle of the most disturbed interval for the period under study, taken when the A_p index reached a value of 207. From the ion drift at 278 km the electric field was estimated to be 225 mV/m for the *top panels* (24.25 UT) and 141 mV/m for the *bottom panels* (24.83 UT)

assumed, the role played by the neutral wind was not too important at *E* region heights. For this reason we first produced scatter plots of the multipulse-derived T_e versus the electric field strength at various *E* region altitudes (Fig. 3a). To estimate the electric field, we used a simple linear interpolation technique when the T_e data was not obtained simultaneously with an electric field measurement. One can see a general trend from Fig. 3a for T_e to increase with electric field strength. There is a central 'cloud' of data points, but the scatter around that cloud can be substantial. Given the discussion in the preceeding section on the unreliability of interpolated electric fields around the times of strongest electric fields we can easily suspect that the electric field determination itself was error prone when large, which would perhaps explain some of the scatter.

On the other hand, we already argued that the electron temperature should depend on the effective electric field and not on the electric field itself. For this reason, we compared the electron *E* region temperatures to the ion temperature around 160 km. The latter was chosen because at that height the T_i response to the effective electric field is the largest [the neutral mass in Eq. (2) being the largest, that is, made mostly of N_2 while $\alpha_i \to 0$]. We first produced scatter plots of the multipulse *E* region electron temperatures versus T_i obtained using the multipulse ion data, averaging the latter over 10 km centered at 160 km. Unfortunately, the result was actually rather noisy. To see if we could clean up the scatter in the T_e vs T_i plots, we then kept the *E*-region electron multipulse data (rather good signal to noise ratio compared to multipulse T_i data higher up), but tried the long pulse T_i data at the 168-km gate instead of the multipulse data. We obtained the results displayed in Fig. 3b. While the multipulse T_i data gave similar trends, the scatter found with the long pulse data was indeed much smaller, most likely owing to its much better signal to noise ratio. As a comparison between Figs. 3a and 3b shows, the data points were also scattered a lot less by using the long pulse T_i data at 168 km than when we used the interpolated electric field.

Partly because of the removal of any interpolation technique and probably also in part because the T_i data depends, like the T_e data, on the effective electric field, and not on the electric field itself, the long pulse low altitude T_i data appeared to be the best at predicting the *E* region electron temperature by showing the least scattering and by getting rid of virtually all low T_e-high electric field cases. However, Fig. 3b clearly shows that this was done at the expense of introducing an 'anomalous branch' in the electron temperature behavior. A discussion of the plausible physics behind such a branch is the topic of the next subsection.

Before moving to an in-depth discussion of Fig. 3b, the reader should also be aware that Fig. 3 was produced by using the second half of the night only, that is, the time interval 22:00–35:00 UT. The first half of the night actually gave similar trends, in fact with an even greater percentage of 'anomalous' data points, but with a greater amount of scattering. We believe from the analysis that follows that this scattering was actually of geophysical origin. We therefore decided to stick with

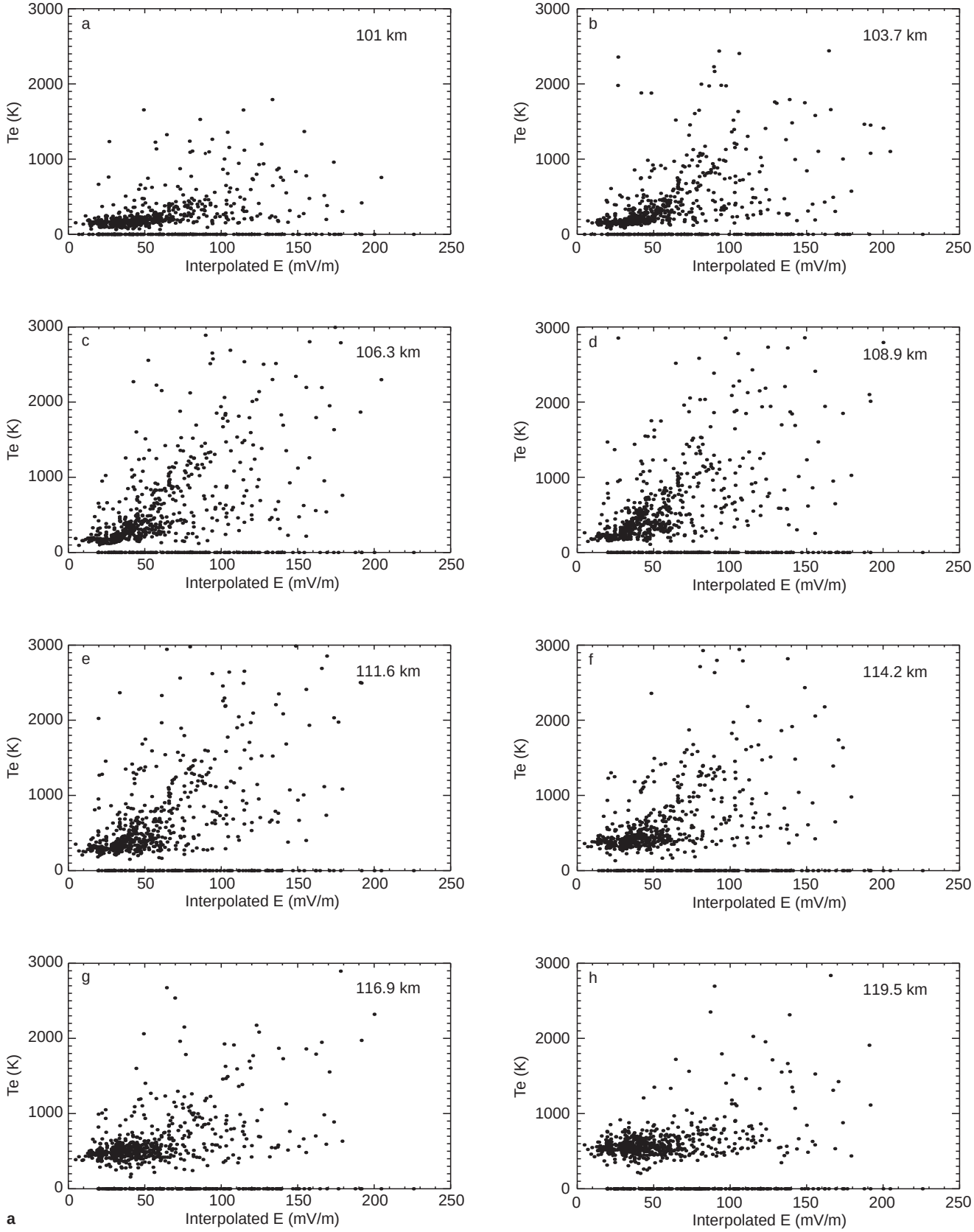

Fig. 3a. Scatter plot of T_e vs E at 8 different altitudes for the time period 22:00 UT to 35:00 UT. The altitudes are 101 km (**a**), 103.7 km (**b**), 106.3 km (**c**), 108.9 km (**d**), 111.6 km (**e**), 114.2 km (**f**), 116.9 km (**g**), and 119.5 km (**h**). Bad data points were given zero values.

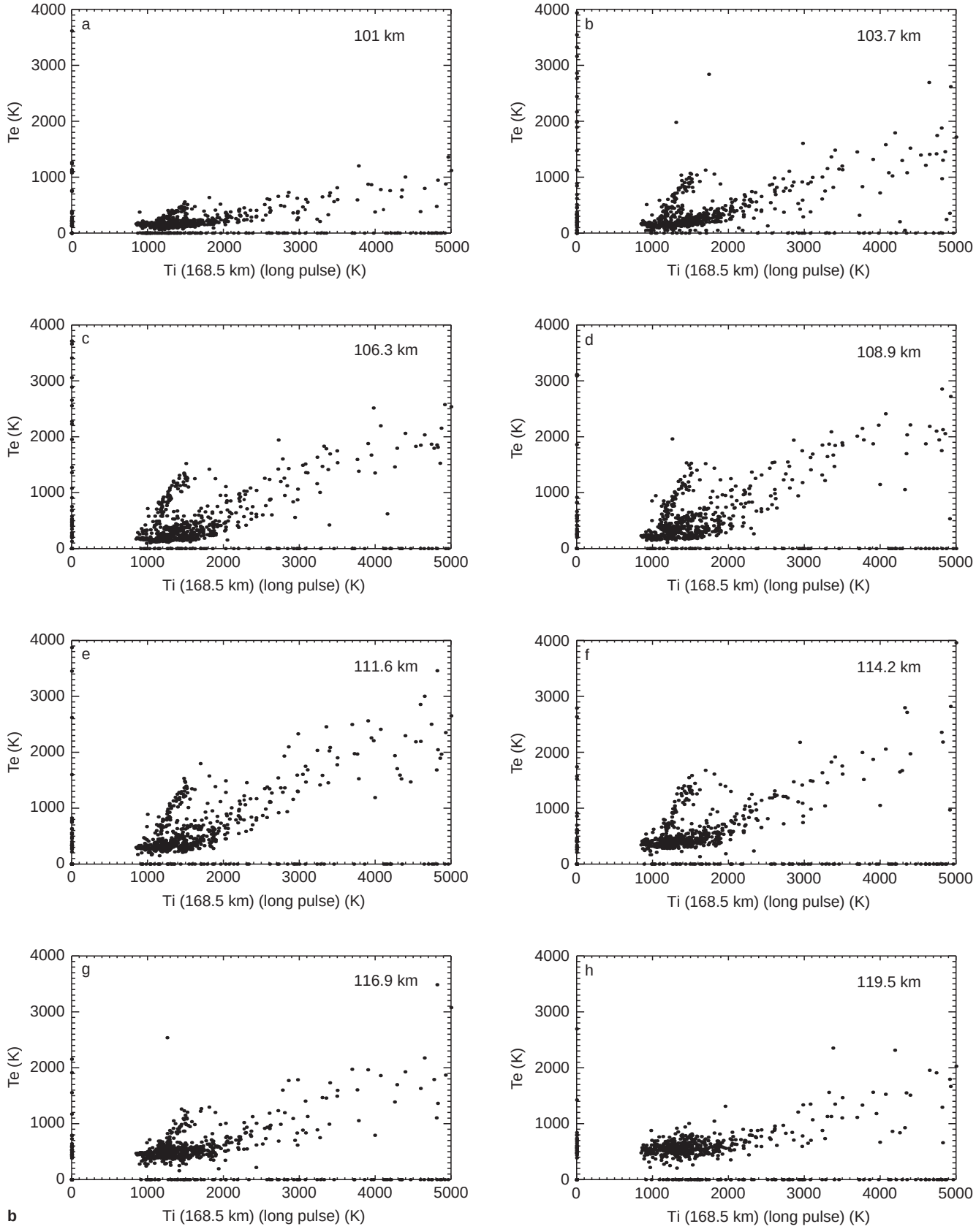

Fig. 3b. Same as Fig. 3a, but with the long-pulse T_i from 168 km replacing the electric field strength

the second half of the night in what follows because of the more unambiguous message that it provided, thanks to its smaller amount of scatter.

4.2 Defining and isolating UTEB events

As was just mentioned, a striking feature of the scatter plots shown in Fig. 3b is the appearance of an 'upper T_e branch' (UTEB) which is clearly noticeable between 101 km and 117 km altitude. The UTEBs form an 'anomaly' not just because they don't behave like the majority of the data, but also because they show electron temperatures that are well above the values that have previously been reported in the literature (as deduced here by taking $T_{i\|}$ and Eq. (3) to find the electric field strength).

The UTEB data did not come from isolated single point measurements. Rather, as might be expected, the data was regrouped around certain UT periods. Figure 4 illustrates this clearly. In Fig. 4, we produced a time sequence of the average T_e between 106 and 116 km (dashed line), the average T_i between 106 and 116 km altitudes (full line) and the average T_i between 140 and 160 km (dash-dot line). The most obvious UTEB event for the displayed time interval started around 33:00 UT and peaked around 34:30 UT. The event was quite clearly taking place while the average T_i around 150 km only suffered a modest increase. In fact, for T_e to have reached more than 1000 K as shown at the peak of the event, T_i at 150 km should have been well in excess of 2000 K, as illustrated by the 'normal' features observed before 29:00 UT (also see the scatter plot in Fig. 3b to confirm this point).

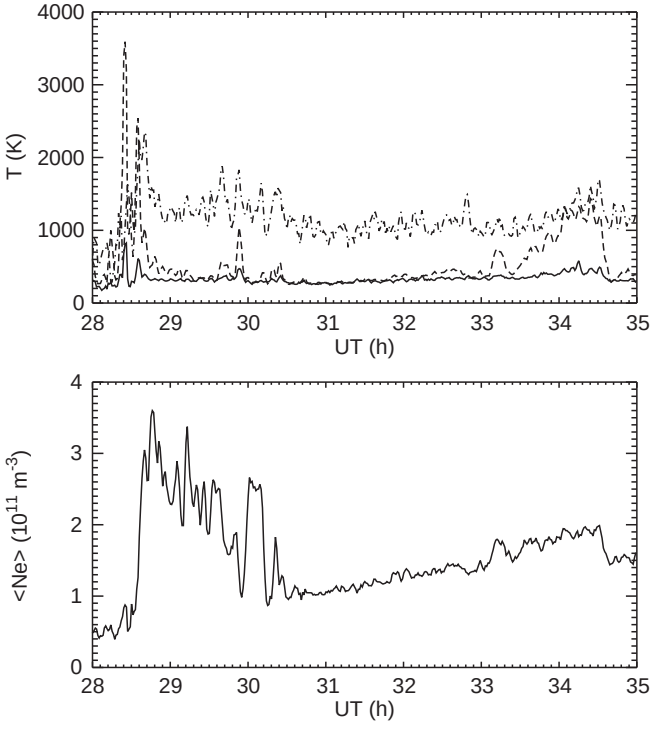

Fig. 4. *Top panel*: time series of $T_{i\|}$ (averaged between 106 and 116 km, *full line*), T_e (averages between 106 and 116 km, *dashed line*) and $T_{i\|}$ (averaged between 140 and 160 km, *dash-dot line*). *Bottom panel*: time series of the electron density averaged between 106 and 116 km

Also shown in Fig. 4 is the average electron density between 106 and 116 km, showing that there was a nice correlation between the 34:00 UT UTEB and the electron density in the same region. This kind of connection should not be viewed as a cause of UTEB, however, but rather as its consequence. The phenomenon has in fact previously been discussed and is due to the reduced recombination rates that one is to expect in the presence of electron production and of electron heating (St.-Maurice *et al.*, 1990; Schlegel, 1982). This is a particularly clearcut example of the phenomenon, since the source of electrons was known rather precisely for the time interval under consideration: detailed model calculations show that photoionization was by far the dominant source of electrons at the time (P.L. Blelly, private communication). This is also easy to see from the steady climb in the background *E* region density starting at about 31:00 UT.

4.3 Neutral winds as the likely origin of UTEBs

Given that the theory of electron heating by plasma waves is not yet fully understood, one could think that the UTEBs might be linked to periods during which the plasma wave generation could have been different, and with it the nonlinear properties of the waves and the associated electron heating (for example, gradients could have somehow become important during the UTEBs in such a way as to change the wave amplitude). However, one could also explain the UTEB generation with the production of strong enough neutral winds in the plasma, thus making the effective electric field altitude-dependent. Based on the detailed observations surrounding UTEB events, we show in the present section that the latter explanation is very likely to be the correct one. This in turn suggests that the electron temperature may well be a robust indicator of the effective electric field strength.

4.3.1 Mean electric field values

The first indication that neutral winds at 150 km are likely the reason for the UTEBs comes from the few electric field measurements that were obtained during UTEBs. To determine these fields we proceeded as follows: we first produced eight 60 K wide T_i bins between 1005 K and 1545 K from the long pulse data (our particular choice of bins was such as to have roughly the same number of samples in each bin, which was typically 8). Next, for each T_i bin we looked at the average interpolated electric field strength that was observed during a UTEB (we picked the 106.3 km altitude in Fig. 3b, but many other altitudes would have

given very similar results) and we compared that mean electric field strength to the mean value read when there was no UTEB for the same T_i interval.

The results of our mean electric field investigation were rather clear: they showed without exception that, for a given T_i bin, the electric fields were much stronger during UTEB events than during normal electron temperature observations. This is illustrated in Fig. 5 where the star symbols give the average electric field strength observed in each of the T_i bins during normal T_e increases, while crosses show the average electric field strength observed during UTEB events (note that we were able to use more T_i bins with the normal data, so that we also plotted results for all bins containing five samples or more in that case). As a reference we also produced in Fig. 5 a theoretical calculation of the parallel ion temperature that one should expect as a function of electric field strength, based on Eq. (3) for $\beta_{\|} = 0.52$, assuming neutral winds could be neglected. For $T_{i\|}$ less than about 1500 K, the normal data set is very close to the value expected in the absence of a neutral wind, while for the UTEB data, $T_{i\|}$ is always much smaller than the expected value. Figure 5 in fact indicates that the electric fields were about 20–25 mV/m greater during UTEBs than during normal events. The conclusion that the UTEB fields were substantially higher also agrees qualitatively with the fact that a closer look at a time series plots of the kind shown in Fig. 4 does show small but perceptible simultaneous increases in T_i near 110 km during UTEBs, but not for normal events. This feature is just as expected from residual frictional heating effects in the presence of larger UTEB electric fields.

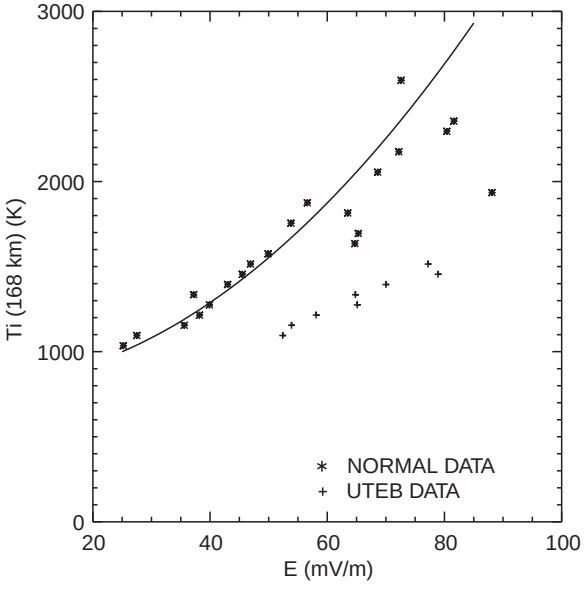

Fig. 5. Parallel ion temperature (long pulse) at 168 km as a function of observed electric field strength for normal events (*star symbols*) and for UTEB events (*crosses*). The long pulse temperatures are 50–100 K greater than the multipulse values. The *full line* gives the computed parallel ion temperature value in the absence of neutral winds

In passing observe that even the "normal" data subset in Fig. 5 shows that the ion temperature falls below the theoretical value once the electric field exceeds 50 mV/m. One reason for this behavior could be the composition changes discussed near the beginning of sect. 3: up to a 7% increase in molecular abundance would translate into a 7% decrease in T_i when analyzing the data with our fixed composition model. The end result, if we applied a 7% increase in $T_{i\|}$, would be a noticeably better agreement with the theoretical line in fact. However, there is a second possibility, in view of the fact that a similar result had been obtained by St.-Maurice and Hanson (1984) using perpendicular ion temperatures in the *F* region above 250 km altitude. The authors attributed this behavior to ion drag, but then just like now, the evidence was only indirect and deduced solely from ion temperature and drift observations. Further insights on this subject can be found in Davies *et al.* (1997) who showed that the ion temperature is, on average, systematically smaller for westward ion flows than for eastward ion flows. In the case of Fig. 5, the ion flow was indeed mostly westward. The reason for the observed asymmetry is rooted in ion drag effects and the mechanism is discussed in (Davies *et al.*, 1997) and (Fuller-Rowell and Rees, 1984). See also a short discussion in the final section of the present paper.

4.3.2 Further inferences from full ion temperature profiles

While Fig. 5 already clearly indicates that T_e around 115 km was reacting to stronger electric fields during UTEB events (while T_i above 150 km was not), the temperature profiles themselves could be used to deduce similar results without the help of an electric field measurement. To this goal, and also to make doubly sure that UTEBs were not caused by unusual composition effects affecting the analysis of the long pulse data, we therefore went back to the multipulse data, used the T_i bins of Fig. 5 and plotted average profiles of T_e and T_i for these bins both for UTEB and for normal events. Figure 6 shows a typical result from this particular approach.

In Fig. 6 the ion temperature from the long pulse was chosen to be in the bin 1365–1425 K at 168 km. Figure 6b shows how the average T_e was changing with altitude for the lower and upper branches, clearly stressing that the only difference between the two T_e data sets had to do with electron heating in the *E* region. By the same token, in Fig. 6a, we see that the ion temperature between 110 and 140 km was also enhanced over the standard set during UTEB events. But, above 140 km, T_i actually decreased for UTEB events, so as to rejoin the standard set and merge with it from 150 km until about 200 km altitude. In the example of Fig. 6 as well as with all other bins studied, note also that above 200 km, T_i once again became larger in the UTEB data set than in the normal data set.

The simplest way to explain the unexpected altitude UTEB ion temperature behavior would be to have large

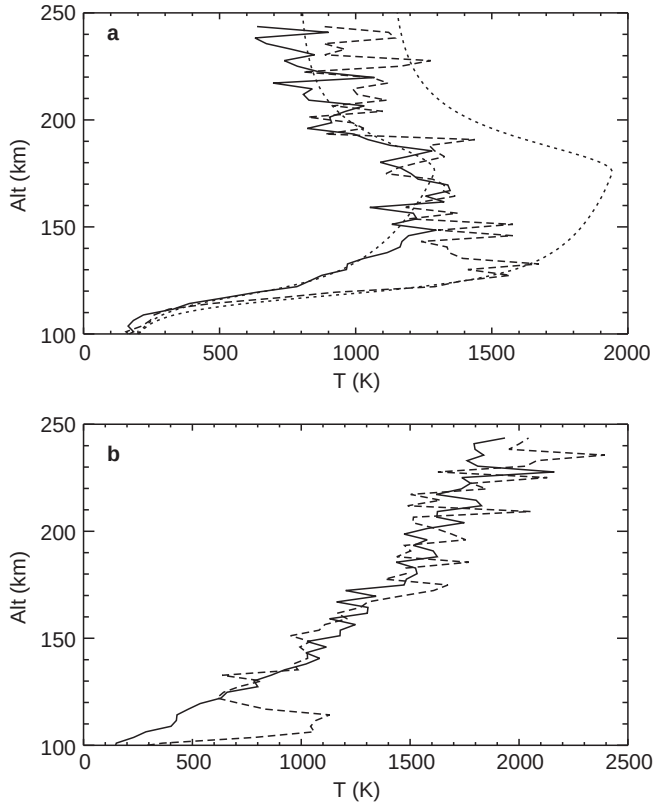

Fig. 6. Average electron (*bottom panel*, **b**) and average parallel ion (*top panel*, **a**) temperature profiles from the multipulse data when the long pulse parallel ion temperature at 168 km was between 1365 K and 1425 K. The UTEB values are given by the *dash lines* and the ordinary average values by the *full lines*. The *dotted lines* in **a** are model values computed using a 775 m/s ion drift for the smaller values and using a 1200 m/s ion drift for the larger values. The model neutral background density value was reduced to 80% of its normal value in both cases

neutral winds along $\mathbf{E} \times \mathbf{B}$ in the UTEB subset for the 150–200 km altitude region. This explanation would be in qualitative agreement with the electric field discussion of sect. 4.3.1 (Fig. 5) in that T_i at 150 km was detectably smaller than indicated by the electric field needed to explain the ion temperatures at lower altitudes, namely, in the 110–120 km region.

For a more quantitative evaluation of the neutral wind hypothesis as it pertains to the ion data, we have also produced theoretical fits of the ion temperatures. Those fits are shown as the pair of dotted lines in Fig. 6a. The fits were obtained as follows: first, we used a single value for the effective electric field $\mathbf{E}'$ at all heights. This means that while we allowed for a neutral wind, we did not let that wind change as a function of height when using Eq. (3) for the various altitudes. We also assumed an exospheric neutral temperature of 1000 K, in addition to using an 80% density multiplication factor in the neutral density model (we used MSIS89, but any standard neutral model would do for the purpose at hand). For the ion parameters, we assumed that the ion population was dominated by NO^+. In our "fit" of the observations we then had to use a magnitude for the $\mathbf{E}' \times \mathbf{B}$ drift of 775 m/s for the 'normal' data subset and 1200 m/s for the UTEB set.

We use the word "fit" between quotes because the model T_i calculations were optimized so as to first and foremost fit the $T_{i\|}$ ramp that starts around 105–110 km altitude. This is where we used the fact that the ions were NO^+, so as to introduce the proper value of the critically important ν_{in}/Ω_i ratio in the model equation. This is also what forced us to adjust the model neutral density by the posted 80% factor. As can be seen from Fig. 6a, we could then get an excellent agreement between the lower model temperature curve and the "normal" ion temperature data not just in the ion temperature ramp between 110 and 130 km, but in fact throughout the entire altitude range. This strongly suggests that under normal conditions, even though some neutral wind must have been blowing, the strength of that neutral wind or its variations of with height were not important as far as the ion energy budget was concerned.

For the UTEB ion temperature fit (the dotted line with the larger values in Fig. 6a), things were different even though we used the same neutral parameters as with the "normal" data subset. While the theoretical calculation did a good job with the temperature ramp, it could of course not accommodate the fact that near 150 km the ion temperature had to go back to the values posted in the normal data set. As we already stressed, the only simple explanation for this decrease was a marked change in the neutral wind by the time we reached 150 km altitude. To be more precise, since the UTEB ion data matched a 775 m/s fit for the magnitude of the $\mathbf{E}' \times \mathbf{B}$ drift at 150 km, we had, at the minimum, to have an increase in the neutral wind component along the electric field direction of $1200 - 775 = 425$ m/s between 120 km and 150 km altitudes, since a 1200 m/s $\mathbf{E}' \times \mathbf{B}$ drift was required to fit the lower altitude T_i data. (It is easy to show that if the magnitude of the $\mathbf{E} \times \mathbf{B}$ drift is much greater than that of the neutral wind, the difference between $|\mathbf{E} \times \mathbf{B}/B^2|$ and $|\mathbf{E}' \times \mathbf{B}/B^2|$ is $|\mathbf{V}_n| \cos\theta$ to leading order. In the context of this approximation, we then refer to the component of the neutral wind along the ion drift direction as the agent responsible for a large discrepancy between $|\mathbf{E} \times \mathbf{B}|$ and $|\mathbf{E}' \times \mathbf{B}|$).

As a further check on our method of analysis, notice that the argument presented above could also have been used in reverse, namely, a 1200 m/s $\mathbf{E}' \times \mathbf{B}$ drift would normally mean that the effective electric field would have had to be about 60 mV/m and that in this case we should have had a parallel ion temperature at 150 km altitude of about 2000 K. This $T_{i\|}$ value was indeed observed at 150 km on our particular night during normal heating events when the 115-km electron temperature was reaching 1000 K (that is, when the effective electric field strength in the electron heating region was indeed 60 mV/m).

In summary, our analysis indicates that around the height at which the electrons were heated during UTEB events (115 km), the effective electric field for the case shown in Fig. 6 was greater by about 20–25 mV/m (i.e. the $\mathbf{E}' \times \mathbf{B}$ drift was greater by 400–500 m/s) during

UTEB events compared to normal events. During the UTEB events, it was consequently not the *E* region electron temperature that was anomalously high, but rather the ion temperature above 130 km that was anomalously low, owing to the presence of strong neutral wind shears above 130 km altitude.

4.3.3 Differences between electric field observations and profile results and implications

While the profile method clearly implies that the electric fields were stronger during UTEB events, the effective electric field that we obtained at the electron heating altitudes (around 115 km) were not necessarily the same as the observed fields and were probably smaller: after all, if large neutral winds were moving along the $\mathbf{E} \times \mathbf{B}$ direction at 150 km, one would suspect that weaker but still possibly large neutral winds should also have been moving along $\mathbf{E} \times \mathbf{B}$ at 115 km. As we now show, this inference was also supported by the data, as seen when we compared the mean electric field values with the values inferred from the profile fitting method.

Our first clue that the UTEB field was greater than deduced from the profile fits comes from a comparison of Fig. 5 with the results inferred from Fig. 6. As seen in Fig. 5, for the particular T_i bin analyzed in Fig. 6, the average measured electric field strength was actually very close to 70 mV/m during UTEB events (while the normal events reported about 45 mV/m). This means that for the UTEB analyzed in Fig. 6 the actual electric field was 10 mV/m greater than the 60 mV/m value (1200 m/s $\mathbf{E}' \times \mathbf{B}$ drift) inferred from the profile method, implying that the neutral wind component along the direction of the ion drift was already of the order of 200 m/s near 115 km altitude, while the sum of that component with the component inferred from the parallel ion temperature was now reaching $200 + 425 = 625$ m/s at 150 km altitude. Since both of these values are surprisingly large for such low altitudes, we decided to compare them against other UTEB results in case of an anomaly with the particular data subset presented in Fig. 6, which comes from just one of seven separate ion temperature bins that we were able to study. We therefore studied the other T_i bins in order to get a more balanced view. The results of this study are presented in Table 1.

In Table 1 the first column lists the centers of the T_i bins that were extracted from the long pulse data at 168 km. The next two columns display the electric fields that were determined using the normal data set and the last two columns the electric fields that were determined using the UTEB data set. For each data set, we used two determinations of the electric field. The first determination shown is directly from the ion drift measurement and is truly a measure of the electric field. The second determination is from the profile method discussed along with Fig. 6. This second field is really a determination of the effective electric field in the ion temperature ramp region, that is, in the 110–120 km altitude range mostly.

Table 1. Electric fields derived for the T_i bins of Fig. 5

$< T_i >$ K	Normal set using $\mathbf{V}_i$ mV/m	Using fit mV/m	UTEB set using $\mathbf{V}_i$ mV/m	Using fit mV/m
1095	28	34	52	41
1155	36	31	54	41
1215	38	30	58	48
1275	40	34	65	55
1335	37	36	65	58
1395	43	39	70	60
1455	46	40	79	66

The second and fourth columns of Table 1 actually correspond to the fields displayed in Fig. 5. The first point to make is that the effective field derived by the profile method are very similar to the observed field for the 'normal' data set. This difference, which indicates systematically smaller profile fields, is small in the normal data set, being of the order of 3 mV/m on average and never exceeding 8 mV/m. We conclude that the effective field was only a few mV/m less than the actual fields, which is equivalent to a neutral wind of the order of 100 m/s or less and is a value to be normally expected around 110–120 km altitude in the *E* region (e.g., Killeen *et al.*, 1992; Kunitake and Schlegel, 1991).

The situation is different for the UTEB subset. Table 1 shows in that case that the difference between observed and profile-derived field is about 11 mV/m on average, reaching at most 13 mV/m. This says that the effective electric field was about 11 mV/m less than the actual field, that is, that there was a neutral wind component of the order of 220 m/s along the ion drift direction around 115 km altitude during UTEB events. This agrees with our discussion of the Fig. 6 results and therefore shows that the results were not a fluke but, rather, agreed well with the rest of the data.

As a further check of the Table 1 results, we also examined the particularly clear UTEB case displayed at the large UT end of Fig. 4. We found in fact the discrepancies between observed and profile-derived fields to be even more pronounced than in Table 1. For the event in question, the UTEB was long-lasting and the electrodynamics far less structured than usual for our specific data set. We could easily determine that during this particular UTEB the electric field reached 90 mV/m at the peak of the event, even though the 150-km parallel ion temperature indicated the field should have been no greater than 55 mV/m while the electron temperature corresponded to what should have been expected for an 80–85 mV/m field. Thus, the electron heating near 115 km altitude indicated a neutral wind component along $\mathbf{E} \times \mathbf{B}$ of the order of 200 m/s at the peak of the event, while the ion temperature at 150 km indicated a 35 mV/m effect, that is, a 700 m/s neutral wind component along $\mathbf{E} \times \mathbf{B}$. These numbers are again in excellent agreement with the discussion of the previous paragraphs.

4.4 Conclusions

We are led to conclude that the major reason for the spectacular alignment of the $T_e(z < 120\,\text{km})$ data with

the $T_i(168\,\mathrm{km})$ data in Fig. 3b, particularly when compared to Fig. 3a, is that both temperatures respond extremely well to the effective electric field and not so much to the electric field itself. Even the UTEB anomaly actually supports this notion. From our study we have found that UTEBs occur when a neutral wind with a strong $\mathbf{E}\times\mathbf{B}$ alignment simultaneously picks up in both altitude regimes, but with a markedly stronger wind at 168 km altitude. This is consistent with the notion of ion drag in a region where viscosity is not yet a dominant term: the neutral wind is then stronger as we go up in altitude because of the smaller neutral mass as we go up. Several numerical studies agree with this notion (e.g., Richmond and Matsushita, 1975; Fuller-Rowell, 1984, 1985; Walterscheid *et al.*, 1985; Mikkelsen *et al.*, 1981; Chang and St.-Maurice, 1991). As for the "normal" data subset, indications are that the neutral wind in that case does not play a major role, being of a smaller, more normal magnitude, and with probably little systematic alignment with the ions as well. Scatter in this part of the data set (Fig. 3b) is nevertheless present and probably reflects in part the presence of remnant neutral wind effects at both altitudes (but probably more so higher up where winds should usually be stronger).

The major consequence from this conclusion is that the electron temperatures, once calibrated, can be used to find the effective electric field whenever that field exceeds 40 mV/m (that is, once the heating effects become measurable). Given that the neutral wind is sometimes not the same below 120 km than above that height, this means that T_e can provide a very useful tool for the study of effective electric fields. Still, one might feel more confident about these results if they could be checked through some independent means first. There was indeed one such means to check the results, and it relied on the multi-altitude drift observations. We now present the results from that part of our investigation, and show that the temperature work could indeed be validated by a careful study of the drift data.

5 Comparison with *E* region measurements of $\mathbf{V}_i$

We have shown in the previous section that, from the point of view of the temperature observations, the case for a very strongly sheared neutral wind flowing along the $\mathbf{E}\times\mathbf{B}$ drift direction during UTEB observations is quite strong. But the multi-altitude ion drift observations discussed in sect. 2 should in principle be able to support this inference. While the multi-altitude range of heights was lower than the region of interest for strong ion heating it had at least the potential to tell us what the neutral wind was doing in the regions where electron heating was taking place.

The determination of neutral winds from multiple altitude measurements along a single magnetic field line is based on a simple manipulation of the ion momentum balance, which reads

$$\mathbf{V}_n = \mathbf{V}_i - \frac{1}{\alpha_i}\left(\frac{\mathbf{V}_i\times\mathbf{B}}{B} + \frac{\mathbf{E}}{B}\right) \tag{4}$$

where $\alpha_i = \nu_{in}/\Omega_i$. The electric field is determined from the measurement of the ion drift vector component perpendicular to $\mathbf{B}$ at 278 km, which yields the $\mathbf{E}\times\mathbf{B}$ drift. The neutral wind determination at any given height then clearly depends on the value of α_i and therefore on the neutral atmosphere because of the proportionality to the ion-neutral collision frequency term. Notice that small uncertainties in α_i can create large uncertainties in the inferred neutral wind when α_i becomes too small. This is the reason for limiting the technique to altitudes 125 km and smaller.

The trouble with using altitude-dependent ion drifts to retrieve neutral winds is that we could only trust measurements that were repeatable. Ion drift variations between consecutive measurement cycles could only indicate that the electric field (or even the neutral wind) was changing while the measurements were made. This would render Eq. (4) useless since the crucial electric field information then becomes unreliable. Unfortunately, as the period under study was extremely active, the electric fields only rarely stayed constant enough over the required 5-min period. In fact, we found only one UTEB instance where the constancy condition was satisfied without question. However, it did happen at a very interesting time, namely, during the peak of the UTEB highlighted in Fig. 4, between 34.17 and 34.34 UT.

For the particular time interval 34.17 to 34.34 UT we proceeded as follows to retrieve both the α_i parameter and the neutral wind vector for the four *E* region altitudes that were available. First we took an average of the parallel ion temperature (and of the electron temperature) during the time interval over which the measurements had been repeatable. Then we used Eq. (4) to get $(\mathbf{V}_n - \mathbf{V}_i)$ in terms of α_i, and then used the observed parallel ion temperature to infer what value of α_i was needed to explain said T_i observations, using Eq. (3).

At the lower altitudes where T_i was relatively small, some special problems arose through a combination of statistical noise and through the fact that T_n had to come from a model (we used MSIS for a 1000 K exospheric temperature). In particular, at 108.9 km we were at first faced with a nominal T_i which was smaller than the model T_n value. We used altitude smoothing, which increased somewhat the T_i value and reduced the model T_n in such a way that the resulting value of α_i provided a smooth interpolation between its two neighbours. The result of our calculations is shown in the first four rows of Table 2. Note that as a check on the sensitivity of the results to our assumption we also ran the isotropic case $\beta_\parallel = 2/3$. The results were a bit different at higher altitudes because of the increasing sensitivity of the neutral wind on α_i when α_i becomes small. In the 124.8-km case the inferred neutral wind increased by about 30%.

The results posted in the upper part of Table 2 are in good agreement with the values inferred from our other approaches. In particular we recover the 60 mV/m (1200 m/s drift) type of effective electric field near 120 km altitude that we had derived from the profile

Table 2. Measured and inferred ionospheric parameters between 34.17 and 34.34 UT, for an 80 mV/m field

Altitude km	East $\mathbf{V}_i$ m/s	North $\mathbf{V}_i$ m/s	$T_{i\|\|}$ K	T_n K	α_i	East $\mathbf{V}_n$ m/s	North $\mathbf{V}_n$ m/s	E'/B m/s	$V_n \cos\theta$ meas m/s	$V_n \cos\theta$ approx m/s
101	−70	−54	205	200	25	−97	−110	1563	144	40
108.9	−113	337	280	210	5	−172	65	1419	116	184
116.9	−617	950	934	345	1.12	−333	186	1224	337	379
124.8	−1055	967	1513	460	0.485	−364	105	1227	339	376
160			1300	775				772		831
278	−1473	632	1532	1100				1495		108

method for the larger T_i bins. However, the electric field itself, at the time for which Table 2 was constructed was just above 80 mV/m, that is, 10 mV/m greater than inferred from the averages discussed in Table 1. This explains why the component of the neutral wind perpendicular to the electric field direction (posted in the next to last column) is closer to 350 m/s than to the 200 m/s that we had estimated by looking at the temperatures alone. As the last column in Table 2 shows, a similar reasoning on temperatures alone for the case posted in Table 2 would have given us an estimate close to 380 m/s in fact (using our $V_n \cos\theta$ approximation to calculate the difference between $|\mathbf{E} \times \mathbf{B}/B^2|$ and $|\mathbf{E}' \times \mathbf{B}/B^2|$). More importantly, Table 2 confirms that the neutral wind was also moving in a direction roughly similar to the ion drift, which is why the ion temperature was smaller than expected even at 125 km. This is illustrated more clearly in Fig. 7, where we are showing the ion drift and inferred neutral drift vectors for the four altitudes that were available. Note that the ion drift at 278 km indicated that the electric field was pointing roughly in the north to north-west direction at the time.

Figure 7 and Table 2 thus show that the higher altitude neutral wind was acquiring a strong westward component. Its magnitude was also increasing very rapidly with altitude, that is, from approximately 150 m/s below 110 km to approximately 380 m/s at 120 km and more than 800 m/s by 160 km altitude.

We conclude this section by commenting on the rest of Table 2. We have added to the table a column giving the value of E'/B. For altitudes below 125 km, that value was determined by solving simultaneously for the

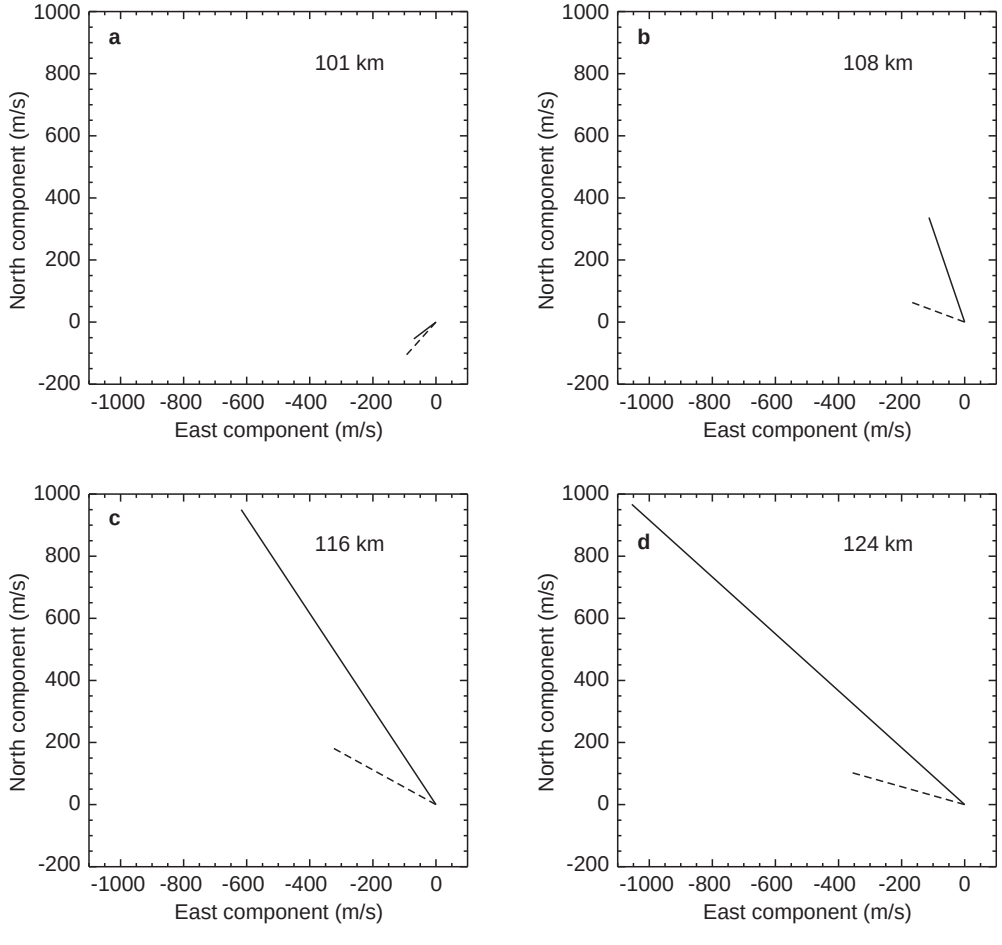

Fig. 7. Ion (*full lines*) and neutral (*dash line*) vectors at 101 (**a**), 108 (**b**), 116 (**c**) and 124 (**d**) km altitudes, derived using multi-position observations and Eq. (2)

momentum and energy balance, using the available observations, as we just described. Higher up, the value of α_i is so small that the ion temperature alone could be used to get E'. We have therefore added the 160 and 278 km altitudes to the table, using the parallel ion temperatures to infer the value of E'/B. Note that owing to uncertainties in the value of $\beta_{\parallel}$ and the exospheric temperature at 278 km, our determination at that height can be uncertain by as much as 150 m/s. Nevertheless, Table 2 clearly shows that, by contrast with the *E* to lower *F* region observations, the magnitude of the effective electric field in the *F* region was remarkably close to the magnitude of the electric field itself. This means that for whatever reason, at least for the UTEBs in the 34 to 35 UT interval, ion drag was able to affect the neutral wind only in the lower *F* region and *E* region.

6 Discussion and conclusion

We have seen that with a detailed study of the ion and electron temperature between 100 and 200 km altitude, we can obtain some very useful information about the neutral wind in the same altitude range when the electric field is strong enough. We found a particularly clear illustration of this for an event that lasted about one hour, and took place around 11 UT on 10 April, 1990. During that event the electric field went up to 90 mV/m while the *E* region electron temperatures and the lower *F* region ion temperatures reacted very differently to the presence of this applied dc electric field. We found that this was attributable to a 350–400 m/s neutral wind around 120 km that rose to about 850 m/s at 160 km altitude and seemed to start to decrease again above 175 km altitude (judging from the differences between the behavior of UTEB versus normal T_i subsets in several plots of the kind displayed in Fig. 6). The strong neutral winds were shown to be flowing in a direction matching the $\mathbf{E} \times \mathbf{B}$ direction by 30° or less.

For the 11 UT (or 35 UT) event that we studied in more detail, we note that the neutral wind direction that we inferred at 160-km altitude would have been close to 90° from what should have been expected for that time of the day if the winds had been driven by pressure gradients. On the one hand, the $\mathbf{E} \times \mathbf{B}$ drift was strongly westward at the time, while the observations were taken just prior to a moderate northward rotation in the flow. This indicates that the plasma was strongly embedded in the evening cell of the convection pattern at the time of the observations (the radar left the morning cell at around 8 MLT). We therefore interpret our result as meaning that in the lower ionosphere the neutrals had been strongly affected by the convection pattern for a prolonged period of time and that they were, as a result, being dragged by the $\mathbf{E} \times \mathbf{B}$ drift of the ions in spite of tidal forces or pressure gradients. On the other hand the pressure gradient forces appeared to have become dominant in the *F* region, since the effective electric field became comparable to the electric field, indicating that ion drag had little effect on the neutral flow.

The behavior that we uncovered here in the lower thermosphere is strongly reminescent of neutral flow signatures derived from ion temperature observations onboard the AE-C satellite at a much later time in the evening convection cell (St.-Maurice and Hanson, 1982). These observations showed that very strong neutral flows could be found on the sunward part of the evening convection cell, in contrast with the morning sector where the neutrals only showed a weak tendency for following the ions when the ion flow turned sunward. This tendancy for strong return flows in the evening cell was also uncovered by modellers and was indeed shown to apply to the *E* region as well (Fuller-Rowell and Rees, 1984); it is attributed to the fact that the Coriolis force can compensate the centripetal acceleration term for a westward flow of a few hundred m/s, leaving the ion drag free to balance tangential acceleration terms. This balance is not possible for an eastward flow, which therefore has trouble being set up. This line of reasoning also explains nicely the ion temperature asymmetries with respect to flow direction that were reported by Davies *et al.* (1997).

As far as the magnitude of the neutral winds that were inferred for the lower *F* region from our work, we note that the vertical shear that was observed, as well as the magnitude of the winds, were consistent with the notion of a sustained ion drag on the neutrals (e.g., Figs. 9 and 10 in Chang and St-Maurice 1991). We would even suggest that it is in fact entirely plausible that the following assumption could be justified during disturbed conditions, that is: whenever there would be evidence for a strong neutral wind in the lower *F* region, it should move primarily in the $\mathbf{E} \times \mathbf{B}$ direction particularly in the evening convection cell.

With regard to a comparison with other observations, we should also note that important altitude variations in the neutral winds right around 115 km have also been detected with TMA trails (e.g. Larsen *et al.*, 1995). This structuring has been attributed to enhanced Hall drag at those altitudes (Larsen and Walterscheid, 1995). Our derived wind magnitudes are also in the same range as those deduced by Thayer (1998) for another exceptional Joule heating event.

From a 'tools' point of view we have been led to the conclusion that during heating events the *E* region electron temperature is as good an effective electric field strength indicator as the ion temperature. During disturbed conditions with lots of dynamical changes, our study indicates that the combined electron and ion temperature studies can be used to get the magnitude of the effective electric field strength over the range of altitudes where Joule heating is taking place. In addition the temperature measurements (in fact, particularly the electron temperature measurements since T_e can be large even at 101 km altitude) can and should be used to complement the *E* region ion drift observations for a determination of the otherwise elusive ion collision frequency on top of the full neutral wind determination.

There are nonetheless some caveats to remember before using the new tools: first of all, from one day to another, or one season to another or even one time

period to another, the electron cooling rates (and therefore the electron temperature response) may well be changing because atomic oxygen can be quite variable at high latitudes particularly in the regions of interest for electron wave heating (e.g. Christensen *et al.*, 1997). A calibration of the electron temperature behavior as a function of electric field during non-UTEB events should therefore be done repeatedly to see if this indeed has an impact on the electron temperature response.

Secondly, the origin and evolution of the plasma waves should in principle be affected at least a little by ambient geophysical parameters such as density gradients and plasma temperatures; in fact rocket observations often see a marked evolution in the wave spectrum through the unstable region, with higher frequency waves at the top of the layer and much lower frequency waves at the bottom (e.g. Pfaff *et al.*, 1992), as if two distinct plasma regimes were present. If so, it would be surprising to find that the wave heating rates would not change at least a little in the process. In fact, it is interesting to note that the shape of the electron temperature profile in the *E* region can also exhibit two peaks on each side of 110 km altitude. This may reflect the presence of the two plasma regimes observed by rockets, or it may simply be that such structures could be caused by neutral wind structures. More studies will be required in order to assess if one of these two possibilities is actually correct.

Acknowledgement. This work has been supported through a grant from the Canadian NSERC. We thank B. Pibaret for her help with the data processing. EISCAT is an international association supported by the research councils of Finland (SA), France (CNRS), the Federal Republic of Germany (MPG), Norway (NAVF), Sweden (NFR) and the United Kingdom (SERC).

Topical Editor D. Alcaydé thanks J. P. Thayer and I. McCrea for their help in evaluating this paper.

Appendix

Effective electric field dependence of the ion and electron heating rates

It may be intuitively obvious that both the ion and electron heating rates in the weakly-ionized ionosphere should depend on the effective electric field $\mathbf{E}'$ and not on the electric field itself since both species are then colliding with the neutral gas. This means that the frame of reference for both species should be the neutral frame of reference. In that frame, the observed field is $\mathbf{E}'$ instead of $\mathbf{E}$.

For the sake of clarity we show explicitly in this appendix how the effective electric field, not the electric field itself, is responsible for the heating of both species.

Ions

The mathematical demonstration that the effective electric field is responsible for the ion heating starts by writing the leading order momentum balance for the ions, namely,

$$\frac{e\mathbf{E}}{m} + \mathbf{V}_i \times \boldsymbol{\Omega}_i = \nu(\mathbf{V}_i - \mathbf{V}_n) \tag{A1}$$

This equation is identical to

$$\frac{e(\mathbf{E} + \mathbf{V}_n \times \mathbf{B})}{m} + (\mathbf{V}_i - \mathbf{V}_n) \times \boldsymbol{\Omega}_i = \nu(\mathbf{V}_i - \mathbf{V}_n) \tag{A2}$$

Using the variable $\mathbf{V}_{in} = \mathbf{V}_i - \mathbf{V}_n$ and the definition of $\mathbf{E}'$, (A2) becomes

$$\frac{e\mathbf{E}'}{m} + \mathbf{V}_{in} \times \boldsymbol{\Omega}_i = \nu\mathbf{V}_{in} \tag{A3}$$

The solution to this equation is

$$\mathbf{V}_{in} = \frac{\alpha_i}{\alpha_i^2 + 1}\frac{\mathbf{E}'}{B} + \frac{1}{\alpha_i^2 + 1}\frac{\mathbf{E}' \times \mathbf{B}}{B^2} \tag{A4}$$

This means that

$$V_{in}^2 = \frac{(E'/B)^2}{\alpha_i^2 + 1} \tag{A5}$$

Substituting this result directly into Eq. (1) of the text immediately gives Eq. (2) of the text.

Electron heating by plasma waves

The relative drift between electrons and neutrals is given by a similar expression for electrons as for ions. In the region of interest, however, $\alpha_e << 1$ and we simply have

$$\mathbf{V}_{en} = \frac{\mathbf{E}' \times \mathbf{B}}{B^2} \tag{A6}$$

If we can assume that the free energy of the plasma waves that heat the electrons below 120 km altitude comes from the relative drift between ions and electrons (certainly the case for Farley-Buneman waves), the power going through the waves should be directly related to the currents, that is to the relative electron-ion drift. However, we can write

$$\mathbf{V}_i - \mathbf{V}_e = \mathbf{V}_{in} - \mathbf{V}_{en} = \frac{\alpha_i}{\alpha_i^2 + 1}\frac{\mathbf{E}'}{B} - \frac{\alpha_i^2}{\alpha_i^2 + 1}\frac{\mathbf{E}' \times \mathbf{B}}{B^2} \tag{A7}$$

From this it is easy to show that the magnitude of the relative ion-electron drift, and therefore the power going through the unstable waves, is related to the magnitude of the relative ion-neutral drift through the relation

$$|\mathbf{V}_i - \mathbf{V}_e| = \alpha_i V_{in} \tag{A8}$$

Thus, for a current-driven instability, the power that goes to the waves depends directly on $\mathbf{E}'$ and not on $\mathbf{E}$. Since the waves are responsible for the heating of the electrons it follows that the electron heating rate must also directly depend on $\mathbf{E}'$ rather than on $\mathbf{E}$.

References

Chang, C. A., and J.-P. St.-Maurice, Two-dimensional high latitude thermospheric modeling; a comparison between moderate and extremely disturbed conditions, *Can. J. Phys.*, **69,** 1007–1031, 1991.

Christensen, A. B., J. H. Hecht, R. L. Walterscheid, M. F. Larsen, and W. E. Sharp, Depletion of oxygen in aurora: evidence for a local mechanism, *J. Geophys. Res.*, **102,** 22,273–22,277, 1997.

Davies, J. A., M. Lester, and I. W. McCrea, A statistical study of ion frictional heating observed by EISCAT, *Ann. Geophys.*, **15,** 1399–1411, 1997.

Fuller-Rowell, T. J., A two-dimensional, high-resolution, nested-grid model of the thermosphere, 1, Neutral response to an electric field "spike", *J. Geophys. Res.*, **89,** 2971–2990, 1984.

Fuller-Rowell, T. J., A two-dimensional, high-resolution, nested-grid model of the thermosphere. 2. Response of the thermosphere to narrow and broad electrodynamic features, *J. Geophys. Res.*, **90,** 6567–6586, 1985.

Fuller-Rowell, T. J., and D. Rees, Interpretation of an anticipated long-lived vortex in the lower thermosphere following simulation of an isolated substorm, *Planet. Space Sci.*, **32,** 69–85, 1984.

Gaimard, P., J.-P. St.-Maurice, C. Lathuillere, and D. Hubert, On the improvement of analytical distributions using recent Monte Carlo results, *J. Geophys. Res.*, **103,** 4079–4095, 1998.

Haldoupis, C., K. Schlegel, and E. Nielsen, Some observations of radio auroral backscatter at 140 MHz during *E* region electron gas heating., *Ann. Geophys.*, **11,** 283–295, 1993.

Hubert, D., and C. Lathuillere, Incoherent scattering of radar waves in the auroral ionosphere in the presence of high electric fields and measurement problems with the EISCAT facility, *J. Geophys. Res.*, **94,** 3653–3662, 1989.

Jones, B., P. J. S. Williams, K. Schlegel, T. Robinson, and I. Haggstrom, Interpretation of enhanced electron temperatures measured in the auroral *E* region during the ERRRIS campaign, *Ann. Geophys.*, **9,** 55–59, 1991.

Killeen, T. L., B. Nardi, P. N. Purcell, R. G. Roble, T.J. Fuller-Rowell, and D. Rees, Neutral winds in the lower thermosphere from Dynamics Explorer 2, *Geophys. Res. Lett.*, **19,** 1093–1096, 1992.

Kissack, R. S., J.-P. St.-Maurice, and D. R. Moorcroft, The effect of electron-neutral energy exchange on the fluid Farley-Buneman instability threshold, *J. Geophys. Res.*, **102,** 24,091–24,115, 1997.

Kofman, W., and C. Lathuillere, Observations by the incoherent scatter technique of the hot spots in the auroral zone ionosphere, *Geophys. Res. Lett.*, **14,** 1158–1161, 1987.

Kofman, W., C. Lathuillere, and B. Pibaret, Neutral atmosphere studies in the altitude range 90–110 km using EISCAT, *J. Atmos. Terr. Phys.*, **48,** 837–847, 1986.

Kunltake, M., and K. Schlegel, Neutral winds in the lower thermosphere at high latitudes from five years of EISCAT data, *Ann. Geophys.*, **9,** 143–155, 1991.

Larsen, M. F., and R. L. Walterscheid, Modified geostrophy in the thermosphere, *J. Geophys. Res.*, **100,** 17,321–17,330, 1995.

Larsen, M. F., T. R. Marshall, I. S. Mikkelsen, B. A. Emery, A. Christensen, D. Kayser, J. Hecht, L. Lyons, and R. Walterscheid, Atmospheric response in aurora experiment: observations of *E* and *F* region neutral winds in a region of postmidnight diffuse aurora, *J. Geophys. Res.*, **100,** 17,299-17,308, 1995.

Lathuillere, C., Ion composition response to auroral energy inputs in the lower *F* region, *Ann. Geophys.*, **5,** 449–454, 1987.

Lathuillere, C., and D. Hubert, Ion composition and ion temperature anisotropy in periods of high electric fields from incoherent scatter observations, *Ann. Geophys.*, **7,** 285–296, 1989.

Lathuillere, C., and B. Pibaret, A statistical model of ion composition in the auroral lower F region, *Adv. Space Res.*, Pergamon Press, **12,** 147–156, 1992.

McCrea, I. W., M. Lester, T. R. Robinson, J.-P. St.-Maurice, N. M. Wade, and T. B. Jones, Derivation of the ion temperature partition coefficients from the study of ion frictional heating events, *J. Geophys. Res.*, **98,** 15,701–15,715, 1993.

Mikkelsen, I. S., T. S. Jorgensen, M. C. Kelley, M. F. Larsen, and E. Pereira, Neutral winds and electric fields in the dusk auroral oval. 2. Theory and model, *J. Geophys. Res.*, **86,** 1525–1536, 1981.

Pfaff, R. F., *et al*., The *E* region rocket/radar instability study (ERRRIS): scientific objectives and campaign overview, *J. Atmos. Terr. Phys.*, **54,** 779–808, 1992.

Rees, M. H., and J. C. G. Walker, Ion and electron heating by electric fields, *Ann. Geophys.*, **24,** 193–197, 1973.

Richmond, A., and S. Matsushita, Thermospheric response to a geomagnetic substorm, *J. Geophys. Res.,* **80,** 2839–2850, 1975.

Robinson, T. R., Towards a self-consistent non-linear theory of radar auroral backscatter, *J. Atmos. Terr. Phys.*, **48,** 417–422, 1986.

Schlegel, K., Reduced effective recombination coefficient in the disturbed polar *E* region, *J. Atmos. Terr. Phys.*, **44,** 183–185, 1982.

Schlegel, K., and J.-P. St.-Maurice, Anomalous heating of the Polar *E* region by unstable plasma waves. I. Observations. *J. Geophys. Res.*, **86,** 1447–1452, 1981.

St.-Maurice, J.-P., Reply, *J. Geophys. Res.*, **92,** 323–327, 1987.

St.-Maurice, J.-P., Electron heating by plasma waves in the high latitude *E* region: theory, *Adv. Space Res.*, Pergamon Press, **10,** 239–249, 1990.

St.-Maurice, J.-P., and W. B. Hanson, Ion frictional heating at high latitudes and its possible use for an in situ determination of neutral thermospheric winds and temperatures. *J. Geophys. Res.*, **87,** 7580–7602, 1982.

St.-Maurice, J.-P., and W. B. Hanson, A statistical study of *F* region ion temperatures at high latitudes based on Atmosphere Explorer C Data, *J. Geophys. Res.*, **89,** 987–996, 1984.

St.-Maurice, J.-P., and R. Laher, Are observed broadband plasma wave amplitudes large enough to explain the enhanced electron temperatures of the high-latitude *E* region?, *J. Geophys. Res.*, **90,** 2843–2850, 1985.

St.-Maurice, J.-P., W. Kofman, and E. Kluzek, Electron Heating by plasma waves in the high latitude *E* region and related effects: Observations, *Adv. Space Res.*, Pergamon Press, **10,** 225–237, 1990.

Thayer, J. P., Height-resolved Joule heating rates in the high-latitude *E* region and the influence of neutral winds, *J. Geophys. Res.*, **103,** 471–487, 1998a.

Thayer, J. P., Radar measurements of the electromagnetic energy rates associated with the dynamic ionospheric load/generator, *Geophys. Res. Lett.*, **25,** 469–472, 1998b.

Walterscheid, R. L., L. R. Lyons, and K. E. Taylor, The perturbed neutral circulation in the vicinity of a symmetric stable auroral arc, *J. Geophys. Res.*, **90,** 12,235–12,248, 1985.

Wickwar, V. B., C. Lathuillere, W. Kofman, and G. Lejeune, Elevated electron temperatures in the auroral *E* layer measured with the Chatanika radar, *J. Geophys. Res.*, **86,** 4721–4730, 1981.

Williams, P. J. S., B. Jones, and G. O. L. Jones, The measured relationship between electric field strength and electron temperature in the auroral *E* region, *J. Atmos. Terr. Phys.*, **54,** 741–748, 1992.

Winkler, E., J.-P. St.-Maurice, and A. R. Barakat, Results from improved Monte Carlo calculations of auroral ion velocity distributions, *J. Geophys. Res.*, **97,** 8399–8423, 1992.